HHS Public Access

Author manuscript

Curr Biol. Author manuscript; available in PMC 2016 October 05.

Published in final edited form as:

Curr Biol. 2015 October 5; 25(19): 2503–2512. doi:10.1016/j.cub.2015.07.065.

An Olfactory Cilia Pattern in the Mammalian Nose Ensures High Sensitivity to Odors

Rosemary C. Challis[1], **Huikai Tian**[1], **Jue Wang**[1], **Jiwei He**[1], **Jianbo Jiang**[2], **Xuanmao Chen**[3], **Wenbin Yin**[1,4], **Timothy Connelly**[1], **Limei Ma**[5], **C. Ron Yu**[5], **Jennifer L. Pluznick**[6], **Daniel R. Storm**[3], **Liquan Huang**[2,7], **Kai Zhao**[2], and **Minghong Ma**[1,*]

[1]Department of Neuroscience, University of Pennsylvania Perelman School of Medicine, Philadelphia, PA 19104, USA

[2]Monell Chemical Senses Center, Philadelphia, PA 19104, USA

[3]Department of Pharmacology, University of Washington School of Medicine, Seattle, WA 98195, USA

[4]Department of Geriatrics, Qilu Hospital of Shandong University, Jinan, Shandong 250012, China

[5]Stowers Institute for Medical Research, Kansas City, MO 64110, USA

[6]Department of Physiology, Johns Hopkins University, Baltimore, MD 21205, USA

[7]College of Life Sciences, Zhejiang University, Hangzhou, Zhejiang 315008, China

Summary

In many sensory organs, specialized receptors are strategically arranged to enhance detection sensitivity and acuity. It is unclear whether the olfactory system utilizes a similar organizational scheme to facilitate odor detection. Curiously, olfactory sensory neurons (OSNs) in the mouse nose are differentially stimulated depending on the cell location. We therefore asked whether OSNs in different locations evolve unique structural and/or functional features to optimize odor detection and discrimination. Using immunohistochemistry, computational fluid dynamics modeling, and patch clamp recording, we discovered that OSNs situated in highly stimulated regions have much longer cilia and are more sensitive to odorants than those in weakly stimulated regions. Surprisingly, reduction in neuronal excitability or ablation of the olfactory G protein in OSNs does not alter the cilia length pattern, indicating that neither spontaneous nor odor-evoked activity is required for its establishment. Furthermore, the pattern is evident at birth, maintained into adulthood, and restored following pharmacologically induced degeneration of the olfactory

[*]Correspondence to: Dr. Minghong Ma, Department of Neuroscience, University of Pennsylvania Perelman School of Medicine, 415 Curie Blvd, CRB Suite 211, Philadelphia, PA 19104-6074. Tel: (215) 746-2790; Fax: (215) 573-9050; minghong@mail.med.upenn.edu.

Author Contributions: Conceptualization, R.C.C., H.T., K.Z., and M.M.; Investigation, R.C.C., H.T., J.W., J.H., J.J., X.C., W.Y., T.C., K.Z., and M.M.; Resources, X.C., L.M., C.R.Y., J.L.P., D.R.S., and L.H.; Writing – Original draft, R.C.C., K.Z., M.M.; Writing – Review & Editing, R.C.C., C.R.Y., L.H., K.Z., and M.M.

See Supplemental Experimental Procedures for details regarding animals and qRT-PCR.

epithelium, suggesting that it is intrinsically programmed. Intriguingly, type III adenylyl cyclase (ACIII), a key protein in olfactory signal transduction and ubiquitous marker for primary cilia, exhibits location-dependent gene expression levels, and genetic ablation of ACIII dramatically alters the cilia pattern. These findings reveal an intrinsically programmed configuration in the nose to ensure high sensitivity to odors.

Graphical Abstract

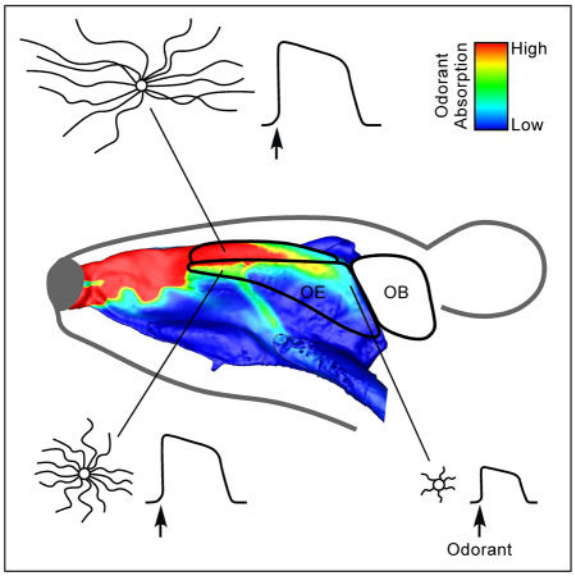

Keywords

olfactory cilia; type III adenylyl cyclase; airflow; odorant absorption; computational fluid dynamics model; patch clamp

Introduction

In order to detect and discriminate a wide variety of stimuli in the environment, sensory organs have developed specialized structures to optimize their functional performance. For example, cone photoreceptors are densely packed in the fovea of the retina to achieve visual acuity, and most sensitive mechanoreceptors with small receptive fields are concentrated in the fingertips for fine touch. However, it is unclear whether the olfactory system uses a similar scheme to facilitate odor detection.

The mouse main olfactory epithelium contains several million olfactory sensory neurons (OSNs), each of which expresses one G protein-coupled odorant receptor (OR) type from a repertoire of ~1200 [1]. A few thousand OSNs expressing the same OR are scattered within one broad zone, while their axons coalesce typically onto two discrete glomeruli (one medial and one lateral) in each olfactory bulb [2, 3]. Odor detection begins when odorants are absorbed into the mucus layer covering the epithelium and bind to ORs on the cilia of OSNs. Odorant binding leads to increased intraciliary cAMP levels via sequential activation of

olfactory G protein (G_{olf}) and type III adenylyl cyclase (ACIII). Subsequent opening of a cyclic nucleotide-gated channel and a Ca^{2+}-activated Cl^- channel depolarizes OSNs, which fire action potentials and transmit odor information to the brain [4].

Olfactory cilia, a hallmark of OSN maturation [5, 6], are essential for OSNs to convert external chemical stimuli into intracellular electrical responses [7, 8]. Each OSN possesses a single dendrite that extends apically and ends in a “knob” at the epithelial surface near the nasal air-mucus interface. From each dendritic knob emanate multiple cilia, which contain the key proteins involved in olfactory signal transduction. Structural and/or functional disruption of olfactory cilia leads to anosmia [9–13], which highlights the importance of these organelles for smell perception.

It has recently become clear that microtubule-based cilia are present in nearly all mammalian cell types and play critical roles in many developmental and physiological processes [14–16]. Defects in cilia formation and/or function lead to ciliopathies, human diseases characterized by symptoms ranging from anosmia and blindness to cystic kidney disorder, brain malformation, obesity, and cognitive deficits [17–20]. Interestingly, cilia in different cell types show distinct morphologies with specific numbers and lengths, suggesting that cilia morphology is under tight biological regulation [21]. The factors that sculpt cilia morphology have begun to emerge in recent years, but it remains unclear how the length of a cilium impacts its function.

By combining fluorescence and electron microscopy, computational fluid dynamics modeling, mouse genetics, and electrophysiology, we report a novel spatial organization of OSNs regarding their cilia length and cell function. OSNs situated in highly stimulated regions have longer cilia and are more sensitive to odorants than those in weakly stimulated regions. Sensory experience and neuronal activity are not required for the establishment and maintenance of the cilia length pattern, but ACIII, a ubiquitous marker for primary cilia, plays a role in this process. These findings have significant implications for both sensory information processing and cilia biology.

Results

Olfactory Cilia Length Depends on the Cell Location in the Olfactory Epithelium

Given the size and geometry of the nasal cavity, OSNs are differentially stimulated depending on the cell location. Cells along the dorsal recess, for example, continuously experience higher airflow rates and odor concentrations than those within the turbinates [22–24]. This prompted us to ask whether cells in different locations evolve unique structural and/or functional features to optimize sensory detection and discrimination. We first examined the morphology of distinct subtypes of OSNs in two different zones: the dorsal zone and the ventral zone from whole-mount olfactory epithelial preparations. We only included cells with sensory cilia, presumably mature OSNs, in our analysis. Using an antibody specific to the MOR28 receptor (Olfr1507 or MOR244-1) [25], we found no systematic difference in the cilia morphology of OSNs in the ventral zone (Figure S1). However, antibody staining against the mOR-EG receptor (Olfr73 or MOR174-9) in the dorsal zone [26] reveals that the cilia length of mOR-EG cells changes systematically with

the cell location (Figures 1A–1C and Table S1); cilia in the anterior septum (Ant) are up to five times longer than those in the posterior septum (Pos). The middle region (Mid) contains cells with intermediate cilia lengths, and the longest cilia are found in the dorsal recess (DR) (Figures 1B and S2). The number of cilia per cell also varies among different regions; for instance, a single cell in the anterior septum has 14.0 ± 2.9 cilia (mean ± SD, n = 43 cells) with similar lengths, versus 5.6 ± 1.8 cilia (n = 47 cells) in the posterior septum, where cells may have more cilia that are too short to be counted. Control experiments indicate that the short cilia are not due to failure of mOR-EG protein transport to the distal cilia (Figure S2). Interestingly, mOR-EG cells along the surface of endoturbinates II–IV do not exhibit dramatic regional differences in cilia length, and most cilia resemble those found in the middle region along the septum (Figure S1).

To test whether the location-dependent cilia length pattern along the septum and dorsal recess applies to OSNs expressing other dorsal zone ORs, we utilized an antibody specific to MOR18-2 (Olfr78) [27], as well as a plant lectin, *Dolichos biflorus* agglutinin (DBA) [28], which labels subsets of OSNs from tens of different OR types [29]. The cilia lengths of MOR18-2 and DBA cells display the same location-dependent pattern as observed with mOR-EG cells (Figure 2 and Table S1). Furthermore, under scanning electron microscopy (SEM), the dorsal recess and anterior septum exhibit the characteristic meshwork of olfactory cilia [8], while the posterior septum reveals much shorter cilia (Figure 1D; see also Figure S2).

Because OSNs in the ventral zone do not display substantial regional differences in cilia length (Figure S1), our subsequent analysis focuses on the cilia pattern within the dorsal zone, specifically along the medial aspect where we observed robust location-dependent changes in cilia length.

The Cilia Pattern Is Positively Correlated With Odorant Absorption

We next asked whether cilia length is correlated with sensory stimulation (e.g., odorant absorption), which also shows location dependence. Because both odorant absorption and cilia length show little regional variation throughout the ventral zone (Figure S1) [24], we restricted our correlation analysis to the dorsal zone where significant regional differences in cilia length are observed. To quantify the cilia pattern, we measured the cilia length of mOR-EG cells along the medial (dorsal recess and septum) and lateral (endoturbinates) aspects of the nasal cavity and generated heatmaps (Figure 3A). To assess odorant absorption in the nasal cavity, we built a 3D computational fluid dynamics model of the mouse nose based on microCT scans from a young adult animal. We simulated a series of parameters under physiological conditions of sniffing and, based on the physicochemical properties of eugenol, a ligand of the mOR-EG receptor, generated a steady state odorant absorption map throughout the nose (Figure 3B). We found a significant positive correlation between the simulated eugenol absorption pattern and the mOR-EG cilia length heatmaps (Figure 3C). Eugenol absorption is highest in the dorsal recess and decreases from the anterior to the posterior nasal cavity due to the gradual reduction of local airflow rates and depletion of odor molecules remaining in the air phase. Odorants with moderate to high mucosal solubility exhibit comparable absorption gradients [24], and because the cilia

pattern applies to multiple OR types (Figures 1 and 2), the correlation suggests that in the dorsal zone OSNs with longer cilia are concentrated in highly stimulated regions of the nose.

The Cilia Pattern Is Established by an Activity-Independent Mechanism

Because of the positive correlation between the cilia pattern and odorant absorption map, we considered whether OSN activation influences cilia length. Cyclic AMP signaling has been reported to positively regulate cilia length in several cell types including OSNs [13, 30, 31]. We therefore asked whether odor-induced cAMP signaling is required for establishing the cilia pattern. We first examined olfactory epithelia from $G\gamma13^{-/-}$ mice, in which Cre-mediated ablation of Gγ13 prevents proper formation and ciliary targeting of G_{olf} in OSNs and eliminates odor-induced electroolfactogram (EOG) signals [32]. Surprisingly, the cilia pattern remains completely intact in these animals (Figure 4A–C and Table S2), suggesting that G_{olf}-mediated activity is not required for the formation and maintenance of the cilia pattern. We also tested the effects of sensory deprivation and dampened neuronal excitability on the cilia pattern by examining the olfactory epithelia from animals that underwent unilateral neonatal naris closure or overexpressed the inward rectifying K^+ channel Kir2.1 [33], respectively. In both cases, the cilia length gradient is preserved; cells in the dorsal recess and anterior septum have much longer cilia than those in the posterior septum (Figure 4D–G and Table S2). Together, these results imply that the cilia pattern is established by an activity-independent mechanism. Moreover, the cilia pattern is established at birth (Figure 5 and Table S2), maintained into adulthood, and restored following regeneration of the olfactory epithelium (Figure S3), suggesting that the pattern is intrinsically programmed.

Genetic Ablation of ACIII Disrupts the Cilia Pattern

Since ACIII is a ubiquitous marker for neuronal cilia [34] and cAMP may regulate olfactory cilia length [13], we considered whether G_{olf}-independent, ACIII-mediated signaling impacts the cilia length of OSNs and examined the cilia pattern in $ACIII^{-/-}$ mice. Remarkably, the pattern is significantly disrupted in these animals (Figure 6A–C and Table S2). Consistent with the notion that ablation of ACIII delays terminal differentiation of OSNs [35], we found that ~30% of labeled cells in knockout mice do not possess cilia. These “bare knobs” are rarely encountered in wild-type mice, especially in regions with long cilia. To minimize the potential developmental effects of ACIII ablation, we only examined cells with cilia, which are presumably mature. The differences in cilia length between the dorsal recess, anterior, and posterior septum are considerably reduced, and cells in these regions are nearly indistinguishable from one another. OSNs in the dorsal recess and anterior septum possess much shorter cilia compared to controls, suggesting that ACIII-mediated signaling plays a role in regulating cilia growth. We then asked whether wild-type animals would have higher *Adcy3* expression levels in areas with longer cilia versus shorter cilia. Using qRT-PCR, we found that the *Adcy3* expression level in the dorsal recess and anterior septum is ~40% higher than that in the posterior septum (Figure 6D). Together, these results reveal that *Adcy3* is correlated with cilia length and may be a required component for the establishment of the cilia pattern, independent of odor-induced activity.

OSNs with Longer Cilia Are More Sensitive to Odorants

To determine if cilia length impacts the function of OSNs, we performed patch clamp recordings on individual OSNs in the intact olfactory epithelium [36] and measured eugenol-induced responses from genetically labeled mOR-EG cells [37]. We first recorded from cells in the dorsal recess and posterior septum since these regions contain OSNs with the longest and shortest cilia, respectively. Compared to posterior cells, OSNs in the dorsal recess showed a lower threshold to eugenol and a larger maximum response at all pulse durations (Figure 7A and B). To test whether OSNs expressing ORs other than mOR-EG exhibit location-dependent differences in odorant sensitivity, we measured odorant-induced responses from randomly selected, unlabeled cells in the dorsal recess and anterior and posterior septum of wild-type mice. As expected, cells in both the dorsal recess and anterior regions showed larger responses to odorants at all pulse lengths compared to those in the posterior region (Figure 7C and D; see also Figure S4). Together, these data support that in the dorsal zone longer cilia render OSNs with higher sensitivity and stronger responses to odor stimulation.

Discussion

This study reveals a novel spatial organization of OSNs in the mouse nose, i.e., OSNs with longer cilia and higher sensitivity have better access to odor molecules. Sensory experience and neuronal activity are not required for establishing the cilia length gradient, which is determined by intrinsic mechanisms. Intriguingly, ACIII exhibits location-dependent gene expression levels, and genetic ablation of ACIII dramatically alters the cilia pattern, independent of odor-induced signaling. These findings offer new insights into peripheral coding and processing of odor information and regulation of cilia morphology and function. Moreover, this work has broad implications for how sensory receptors optimize detection sensitivity in various physiological contexts.

Spatial Organization in the Main Olfactory Epithelium

The zonal organization of OR gene expression in the rodent nose has prompted active investigation into a potential spatial component in peripheral olfactory coding. According to the “sorption theory”, the physicochemical properties of odorants (e.g., volatility and water solubility) influence their spatial absorption across the main olfactory epithelium [24, 38–40]. Hydrophilic molecules, which are highly absorptive and better retained in the aqueous mucus, are deposited in the dorsal zone along the medial aspect of the nose where the airflow reaches first. Hydrophobic molecules, on the other hand, are less absorptive and uniformly deposited throughout the dorsal and ventral zones in both the medial and lateral regions [24]. Here, we describe a spatial organization in which olfactory cilia length depends on OSN location in the olfactory epithelium. The dorsal zone exhibits a robust cilia length gradient that is positively correlated with odorant absorption (Figure 3). The ventral zone, however, shows no location-dependent changes in cilia length (Figure S1), presumably suited for detecting hydrophobic odorants, which exhibit a relatively flat absorption pattern [24].

Within the dorsal zone, OSNs expressing the same OR along the medial and lateral regions target medial and lateral glomeruli, respectively [41]. Generally, OSNs in the dorsal recess and septum innervate medial glomeruli, while those along and within the turbinates innervate lateral glomeruli. Dorsal zone OSNs with very long cilia are only observed in the dorsal recess and anterior septum (Figures 1 and 2), a finding that may contribute to a previously reported medial-lateral timing difference in olfactory bulb neurons [42].

The most dramatic difference in cilia length is found along the medial aspect of the dorsal zone; i.e., a single medial glomerulus receives inputs from OSNs that are heterogeneous in their cilia lengths (Figures 1–3). Patch clamp analysis reveals that OSNs in the dorsal recess and anterior septum (with longer cilia) are more sensitive to odorants compared to cells in the posterior septum (with shorter cilia) (Figure 7). This can be explained by the fact that longer cilia have a larger surface area for contacting odors. Based on the cable theory, the length constant of olfactory cilia is estimated to be ~220 μm when the membrane is not leaky (i.e., with negligible channel opening). This suggests that upon stimulation by faint odors, the electrical signals generated along a long cilium can travel far enough to the cell body and contribute to membrane depolarization. Due to spatial summation, cells with longer cilia would show a higher sensitivity and larger response to low concentrations of odors. Conceivably, placing OSNs with longer cilia in highly stimulated regions would increase their chance of encountering faint odors and boost the sensitivity of the system.

Compared to their long-cilia counterparts, short-cilia cells have a higher response threshold and are less likely to reach saturation, making them better suited for coding intensity differences at higher concentrations. Therefore, placing OSNs with shorter cilia in the posterior septum, which is only reached by strong odor stimuli, would ensure a broad dynamic range of the system. If these neurons were designed to carry redundant information, OSNs in the posterior septum should grow longer cilia to compensate for weaker stimulation. Our work reveals the opposite scenario, suggesting that the peripheral olfactory system is spatially organized to match cell sensitivity with the incoming stimuli, adding a new dimension to the “sorption theory”.

Regulation of Olfactory Cilia Length and the Cilia Pattern

Contrary to the common belief that OSNs have rather uniform morphology, we demonstrate that OSNs are intrinsically programmed to grow longer or shorter cilia depending on their location in the olfactory epithelium. Intriguingly, the cilia length gradient is observed throughout development, after regeneration, or following sensory deprivation or elimination of spontaneous and evoked OSN activity (Figures 4, 5, and S3). These findings exclude a number of factors possibly involved in regulating the formation and maintenance of the cilia pattern (i.e., the length gradient).

Genetic ablation of ACIII disrupts the cilia pattern (Figure 6), revealing a potential role of ACIII in regulating cilia length and the establishment of the cilia pattern. Curiously, G_{olf}-dependent activity is not required for the cilia length gradient, suggesting that ACIII acts via a G_{olf}-independent mechanism. It is possible that odor-induced intracellular cAMP changes are transient and not sufficient to impact the cilia pattern, but ligand-independent ACIII activity may cause sustained cAMP elevation to affect cilia growth and maintenance.

Although we cannot rule out the possibility that ablation of ACIII sequesters some OSNs at a developmentally delayed stage [35], thus preventing the growth of longer cilia, our finding is consistent with a previously reported role of cAMP in mediating olfactory cilia length [13]. Given that ciliary localization of ACIII is not required for cilia growth [43], the pattern may be the result of intrinsic, location-dependent regulation of *Adcy3* gene expression, leading to differential cAMP levels and transcription of downstream cilia proteins. This is supported by the fact that *Adcy3* expression is higher in regions with longer cilia versus shorter cilia (Figure 6). The positive correlation between ACIII levels and cilia length is also observed following sensory deprivation, which results in upregulation of ACIII mRNA and protein levels [44, 45] and increased cilia length in all regions throughout the epithelium (Figure 4). These data support the ACIII$^{-/-}$ phenotype and a potential causal link between ACIII and cilia length. Interestingly, pharmacological inhibition of ACIII has been reported to increase primary cilia length in certain cell types [46]. This apparently conflicting finding may be because (1) ACIII has differential effects on various cell types and/or (2) the pharmacological treatments affect molecular targets other than ACIII.

A number of molecules (cAMP, Centrin2, Goofy, and Bardet-Biedl syndrome, intraflagellar transport, and Meckel Gruber syndrome proteins) play critical roles in the formation and/or maintenance of olfactory cilia [9, 11–13, 27, 47, 48]. Disruption of these cilia-related proteins results in abnormal ACIII expression and shortened, malformed, or absent olfactory cilia. Whether or not these factors show location-dependent expression and are involved in the establishment of the cilia pattern remains to be determined. Interestingly, *Adcy3* expression is comparable between the dorsal recess and anterior septum (Figure 6), even though these regions exhibit different cilia lengths, indicating that additional molecules may contribute to the location-dependent regulation of cilia length. Together, it is likely that the formation and maintenance of the cilia pattern is governed by multiple factors, which remain to be identified in future investigations.

Experimental Procedures

Immunohistochemistry

Following fixation, the nasal septum or turbinates were dissected out *en bloc* and processed for antibody staining. Olfactory mucosa were peeled away from the underlying bone and mounted in Vectashield mounting medium (Vector Laboratories). Images (z-step = 1 μm) were taken under a Leica TCS SP5 II confocal microscope (Leica Microsystems, Buffalo Grove, IL, USA) with a 40x oil objective. Cilia were traced using Leica LAS AF Lite software. See Supplemental Experimental Procedures for more details regarding immunohistochemistry, regional subdivisions, cilia length quantification, and SEM.

Computational Fluid Dynamics Model

An anatomically accurate 3D nasal model was constructed with a total of 1.8×10^7 cells in order to completely resolve the airspace and the boundary layer where odorant molecules become trapped. The nasal wall was assumed to be rigid and smooth, with no slip condition (zero velocity). Uniform velocity was specified at the inlet, while pressure outlet was used at the pharynx. Airflow was assumed to be quasi-steady, laminar, incompressible, and

Newtonian. Finally, the steady state odorant deposition through airflow and mucosal uptake of vaporized eugenol was simulated based on the calculated airflow field and estimated physicochemical properties. See Supplemental Experimental Procedures for more details on the model and correlation analysis.

Patch Clamp Recordings and Dose Response Curves

Intact epithelia were prepared and the dendritic knobs of OSNs were visualized and recorded as in our published procedures (see Supplemental Experimental Procedures for details). A glass pipette was used to deliver stimuli by pressure ejection (20 psi or 138 kPa) through a picospritzer (Pressure System IIe, Fairfield, NJ, USA) at different pulse lengths (0 to 400 ms). Longer pulses elicited larger responses in all cells due to higher concentrations reaching the recording site. Dose response curves were fit by the Hill equation: $V=V_{max}/(1+(K_{1/2}+C)^{n})$, where V represents the peak receptor potential, V_{max} the maximum response at the saturating pulse length, $K_{1/2}$ the pulse length at which half of the maximum response was reached, C the pulse length and n the Hill coefficient. Only cells tested at a minimum of three pulse lengths were included in the analysis. Eugenol (Sigma) and the odorant mixture (see Supplemental Experimental Procedures) were prepared as 0.5 M solutions in DMSO and kept at −20°C. Final solutions were prepared before each experiment by adding Ringer's.

Supplementary Material

Refer to Web version on PubMed Central for supplementary material.

Acknowledgments

We are grateful to Drs. Yoshihiro Yoshihara and Gilad Barnea for generously providing the antibodies against mOR-EG and MOR28, respectively. We thank Penn Vet Imaging Core (supported by the National Center for Research Resources 1S10RR024583) for obtaining microCT scans of the mouse nasal cavity and Drs. Dewight Williams and Ray Meade at the Penn Electron Microscopy Resource Laboratory for performing scanning EM experiments. We thank Hugh Huang and Marina Zhang for their help in quantification of cilia lengths, and Dr. Wenqin Luo's lab for helpful discussions. This work was supported by grants from the NIDCD, NIH (F31DC013945 to R.C.C., R01DC011554 and R01DC006213 to M.M., R03DC008187 to K.Z., and R21DC013177 to L.H.).

References

1. Zhang X, Zhang X, Firestein S. Comparative genomics of odorant and pheromone receptor genes in rodents. Genomics. 2007; 89:441–450. [PubMed: 17303377]
2. Mombaerts P. Axonal wiring in the mouse olfactory system. Annu Rev Cell Dev Biol. 2006; 22:713–737. [PubMed: 17029582]
3. Mori K, Sakano H. How is the olfactory map formed and interpreted in the mammalian brain? Annu Rev Neurosci. 2011; 34:467–499. [PubMed: 21469960]
4. Su CY, Menuz K, Carlson JR. Olfactory perception: receptors, cells, and circuits. Cell. 2009; 139:45–59. [PubMed: 19804753]
5. Schwarzenbacher K, Fleischer J, Breer H. Formation and maturation of olfactory cilia monitored by odorant receptor-specific antibodies. Histochem Cell Biol. 2005; 123:419–428. [PubMed: 15868179]
6. Menco BP, Farbman AI. Genesis of cilia and microvilli of rat nasal epithelia during pre-natal development. II Olfactory epithelium, a morphometric analysis. J Cell Sci. 1985; 78:311–336. [PubMed: 4093476]

7. Menco BP. Ultrastructural aspects of olfactory signaling. Chem Senses. 1997; 22:295–311. [PubMed: 9218142]
8. McEwen DP, Jenkins PM, Martens JR. Olfactory cilia: our direct neuronal connection to the external world. Curr Top Dev Biol. 2008; 85:333–370. [PubMed: 19147011]
9. Kulaga HM, Leitch CC, Eichers ER, Badano JL, Lesemann A, Hoskins BE, Lupski JR, Beales PL, Reed RR, Katsanis N. Loss of BBS proteins causes anosmia in humans and defects in olfactory cilia structure and function in the mouse. Nat Genet. 2004; 36:994–998. [PubMed: 15322545]
10. McEwen DP, Koenekoop RK, Khanna H, Jenkins PM, Lopez I, Swaroop A, Martens JR. Hypomorphic CEP290/NPHP6 mutations result in anosmia caused by the selective loss of G proteins in cilia of olfactory sensory neurons. Proc Natl Acad Sci USA. 2007; 104:15917–15922. [PubMed: 17898177]
11. McIntyre JC, Davis EE, Joiner A, Williams CL, Tsai IC, Jenkins PM, McEwen DP, Zhang L, Escobado J, Thomas S, et al. Gene therapy rescues cilia defects and restores olfactory function in a mammalian ciliopathy model. Nat Med. 2012; 18:1423–1428. [PubMed: 22941275]
12. Tadenev AL, Kulaga HM, May-Simera HL, Kelley MW, Katsanis N, Reed RR. Loss of Bardet-Biedl syndrome protein-8 (BBS8) perturbs olfactory function, protein localization, and axon targeting. Proc Natl Acad Sci USA. 2011; 108:10320–10325. [PubMed: 21646512]
13. Kaneko-Goto T, Sato Y, Katada S, Kinameri E, Yoshihara S, Nishiyori A, Kimura M, Fujita H, Touhara K, Reed RR, et al. Goofy coordinates the acuity of olfactory signaling. J Neurosci. 2013; 33:12987–12996. [PubMed: 23926254]
14. Louvi A, Grove EA. Cilia in the CNS: the quiet organelle claims center stage. Neuron. 2011; 69:1046–1060. [PubMed: 21435552]
15. Berbari NF, O'Connor AK, Haycraft CJ, Yoder BK. The primary cilium as a complex signaling center. Curr Biol. 2009; 19:R526–535. [PubMed: 19602418]
16. Guemez-Gamboa A, Coufal NG, Gleeson JG. Primary cilia in the developing and mature brain. Neuron. 2014; 82:511–521. [PubMed: 24811376]
17. Jenkins PM, McEwen DP, Martens JR. Olfactory cilia: linking sensory cilia function and human disease. Chem Senses. 2009; 34:451–464. [PubMed: 19406873]
18. Hildebrandt F, Benzing T, Katsanis N. Ciliopathies. N Engl J Med. 2011; 364:1533–1543. [PubMed: 21506742]
19. Sheffield VC. The blind leading the obese: the molecular pathophysiology of a human obesity syndrome. Trans Am Clin Climatol Assoc. 2011; 121:172–181. [PubMed: 20697559]
20. Valente EM, Rosti RO, Gibbs E, Gleeson JG. Primary cilia in neurodevelopmental disorders. Nat Rev Neurol. 2014; 10:27–36. [PubMed: 24296655]
21. Ishikawa H, Marshall WF. Ciliogenesis: building the cell's antenna. Nat Rev Mol Cell Biol. 2011; 12:222–234. [PubMed: 21427764]
22. Yang GC, Scherer PW, Zhao K, Mozell MM. Numerical modeling of odorant uptake in the rat nasal cavity. Chem Senses. 2007; 32:273–284. [PubMed: 17220517]
23. Kimbell JS, Godo MN, Gross EA, Joyner DR, Richardson RB, Morgan KT. Computer simulation of inspiratory airflow in all regions of the F344 rat nasal passages. Toxicol Appl Pharmacol. 1997; 145:388–398. [PubMed: 9266813]
24. Scott JW, Sherrill L, Jiang J, Zhao K. Tuning to odor solubility and sorption pattern in olfactory epithelial responses. J Neurosci. 2014; 34:2025–2036. [PubMed: 24501345]
25. Barnea G, O'Donnell S, Mancia F, Sun X, Nemes A, Mendelsohn M, Axel R. Odorant receptors on axon termini in the brain. Science. 2004; 304:1468. [PubMed: 15178793]
26. Kaneko-Goto T, Yoshihara S, Miyazaki H, Yoshihara Y. BIG-2 mediates olfactory axon convergence to target glomeruli. Neuron. 2008; 57:834–846. [PubMed: 18367085]
27. Pluznick JL, Rodriguez-Gil DJ, Hull M, Mistry K, Gattone V, Johnson CA, Weatherbee S, Greer CA, Caplan MJ. Renal cystic disease proteins play critical roles in the organization of the olfactory epithelium. PLoS ONE. 2011; 6:e19694. [PubMed: 21614130]
28. Lipscomb BW, Treloar HB, Greer CA. Cell surface carbohydrates reveal heterogeneity in olfactory receptor cell axons in the mouse. Cell Tissue Res. 2002; 308:7–17. [PubMed: 12012202]

29. Lipscomb BW, Treloar HB, Klenoff J, Greer CA. Cell surface carbohydrates and glomerular targeting of olfactory sensory neuron axons in the mouse. J Comp Neurol. 2003; 467:22–31. [PubMed: 14574677]
30. Besschetnova TY, Kolpakova-Hart E, Guan Y, Zhou J, Olsen BR, Shah JV. Identification of signaling pathways regulating primary cilium length and flow-mediated adaptation. Curr Biol. 2010; 20:182–187. [PubMed: 20096584]
31. Abdul-Majeed S, Moloney BC, Nauli SM. Mechanisms regulating cilia growth and cilia function in endothelial cells. Cell Mol Life Sci. 2012; 69:165–173. [PubMed: 21671118]
32. Li F, Ponissery-Saidu S, Yee KK, Wang H, Chen ML, Iguchi N, Zhang G, Jiang P, Reisert J, Huang L. Heterotrimeric G protein subunit Ggamma13 is critical to olfaction. J Neurosci. 2013; 33:7975–7984. [PubMed: 23637188]
33. Yu CR, Power J, Barnea G, O'Donnell S, Brown HE, Osborne J, Axel R, Gogos JA. Spontaneous neural activity is required for the establishment and maintenance of the olfactory sensory map. Neuron. 2004; 42:553–566. [PubMed: 15157418]
34. Bishop GA, Berbari NF, Lewis J, Mykytyn K. Type III adenylyl cyclase localizes to primary cilia throughout the adult mouse brain. J Comp Neurol. 2007; 505:562–571. [PubMed: 17924533]
35. Lyons DB, Allen WE, Goh T, Tsai L, Barnea G, Lomvardas S. An epigenetic trap stabilizes singular olfactory receptor expression. Cell. 2013; 154:325–336. [PubMed: 23870122]
36. Grosmaitre X, Vassalli A, Mombaerts P, Shepherd GM, Ma M. Odorant responses of olfactory sensory neurons expressing the odorant receptor MOR23: a patch clamp analysis in gene-targeted mice. Proc Natl Acad Sci USA. 2006; 103:1970–1975. [PubMed: 16446455]
37. Oka Y, Katada S, Omura M, Suwa M, Yoshihara Y, Touhara K. Odorant receptor map in the mouse olfactory bulb: in vivo sensitivity and specificity of receptor-defined glomeruli. Neuron. 2006; 52:857–869. [PubMed: 17145506]
38. Kent PF, Mozell MM, Murphy SJ, Hornung DE. The interaction of imposed and inherent olfactory mucosal activity patterns and their composite representation in a mammalian species using voltage-sensitive dyes. J Neurosci. 1996; 16:345–353. [PubMed: 8613801]
39. Schoenfeld TA, Cleland TA. Anatomical contributions to odorant sampling and representation in rodents: zoning in on sniffing behavior. Chem Senses. 2006; 31:131–144. [PubMed: 16339266]
40. Scott JW. Sniffing and spatiotemporal coding in olfaction. Chem Senses. 2006; 31:119–130. [PubMed: 16354743]
41. Schoenfeld TA, Cleland TA. The anatomical logic of smell. Trends in neurosciences. 2005; 28:620–627. [PubMed: 16182387]
42. Zhou Z, Belluscio L. Coding odorant concentration through activation timing between the medial and lateral olfactory bulb. Cell Rep. 2012; 2:1143–1150. [PubMed: 23168258]
43. McIntyre JC, Joiner AM, Zhang L, Iniguez-Lluhi J, Martens JR. SUMOylation regulates ciliary localization of olfactory signaling proteins. J Cell Sci. 2015; 128:1934–1945. [PubMed: 25908845]
44. Coppola DM, Waggener CT. The effects of unilateral naris occlusion on gene expression profiles in mouse olfactory mucosa. J Mol Neurosci. 2012; 47:604–618. [PubMed: 22187364]
45. He J, Tian H, Lee AC, Ma M. Postnatal experience modulates functional properties of mouse olfactory sensory neurons. Eur J Neurosci. 2012; 36:2452–2460. [PubMed: 22703547]
46. Ou Y, Ruan Y, Cheng M, Moser JJ, Rattner JB, van der Hoorn FA. Adenylate cyclase regulates elongation of mammalian primary cilia. Exp Cell Res. 2009; 315:2802–2817. [PubMed: 19576885]
47. Ying G, Avasthi P, Irwin M, Gerstner CD, Frederick JM, Lucero MT, Baehr W. Centrin 2 is required for mouse olfactory ciliary trafficking and development of ependymal cilia planar polarity. J Neurosci. 2014; 34:6377–6388. [PubMed: 24790208]
48. Williams CL, McIntyre JC, Norris SR, Jenkins PM, Zhang L, Pei Q, Verhey K, Martens JR. Direct evidence for BBSome-associated intraflagellar transport reveals distinct properties of native mammalian cilia. Nat Commun. 2014; 5:5813. [PubMed: 25504142]

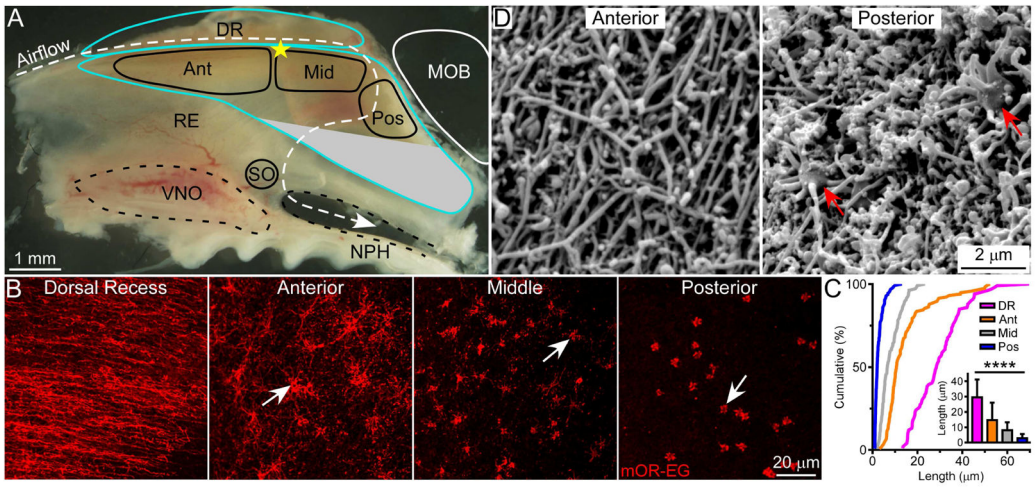

Figure 1. Olfactory Cilia Length Depends on the Cell Location in the Olfactory Epithelium

(**A**) Subdivision of the dorsal zone of the mouse nasal septum. The olfactory epithelium is outlined in blue. The white dashed line marks the dorsal airstream during inspiration. No mOR-EG cells are found in the gray region, which is outside of the dorsal zone. Ant = anterior; Mid = middle; Pos = posterior; DR = dorsal recess. MOB = main olfactory bulb; NPH = nasopharynx; RE = respiratory epithelium; SO = septal organ; VNO = vomeronasal organ. The yellow star denotes the most dorsal point where the nasal septal cartilage meets the ethmoid bone and was used to facilitate comparisons between tissues (see Supplemental Experimental Procedures). (**B**) Whole-mount olfactory epithelia were stained with the mOR-EG antibody (n = 10 animals). Confocal images were taken from the four different regions shown in (A). Arrows mark dendritic knobs, which in areas with longer cilia, are presumably covered by ciliary mesh (see also Figure 2 and Figure S2). (**C**) Cumulative frequency (%) of cilia length from mOR-EG cells in the dorsal recess (magenta), anterior (orange), middle (gray), and posterior (blue) regions. The bar graph shows quantification of cilia length (mean ± SD); Tukey's multiple comparisons test, **** $p < 0.0001$. (**D**) Surface SEM images were taken from the anterior and posterior septum (n = 3 animals). See also Figure S1, S2 and Table S1.

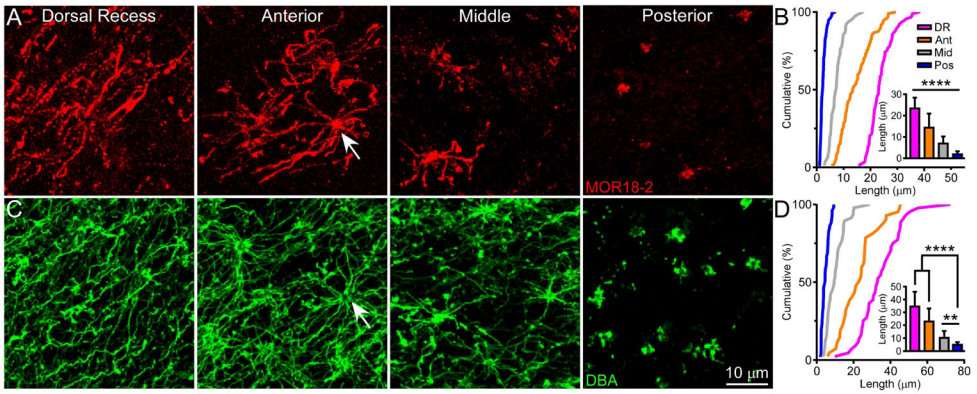

Figure 2. The Cilia Length Pattern Applies to OSNs Expressing Other OR Types

(**A**) Whole-mount olfactory epithelia were stained with the MOR18-2 antibody (n = 5 animals). Confocal images were taken from the dorsal recess, anterior, middle, and posterior septum. The arrow marks a dendritic knob. (**B**) Cumulative frequency (%) of cilia length from MOR18-2 cells in all four regions. The bar graph shows quantification of cilia length (mean ± SD); Tukey's multiple comparisons test, **** $p < 0.0001$. (**C**) Whole-mount olfactory epithelia were stained with DBA (n = 16 animals stained with DBA alone or combined with either the mOR-EG or MOR18-2 antibody) and images were taken as in (A). (**D**) Cumulative frequency (%) of cilia length from DBA^+ cells in all four regions. The bar graph shows quantification of cilia length (mean ± SD); Tukey's multiple comparisons test, ** $p < 0.01$, **** $p < 0.0001$. See also Figure S2 and Table S1.

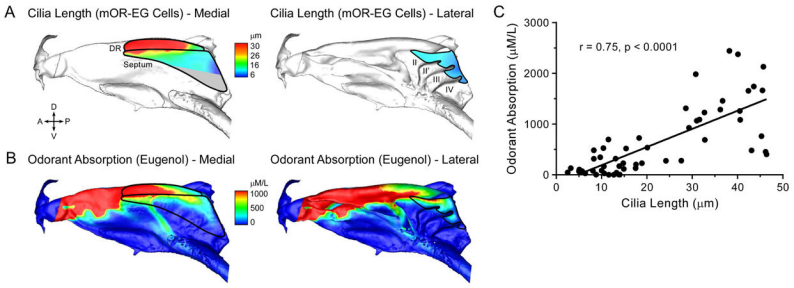

Figure 3. The Cilia Pattern Is Positively Correlated With Odorant Absorption

The solid black lines mark the contour of the olfactory epithelium along the medial (dorsal recess and septum) and lateral (endoturbinates) aspects of the dorsal zone. A = anterior; D = dorsal; P = posterior; V = ventral. (**A**) Cilia length heatmaps. There are no mOR-EG cells in the gray region. (**B**) Computational simulation of eugenol absorption along the medial and lateral aspects of the nasal cavity. The nasal airflow simulation assumes steady-state inspiration at 100 mL/min (sniffing state for mouse) with a non-saturating eugenol concentration of 100 ppm in the inspired air. Odorant absorption (μM/L) is linearly scaled to the incoming odorant concentration up to ~10,000 ppm, which is beyond the typical range of odor stimulation. (**C**) Odorant absorption values are plotted versus the corresponding average cilia length in each location. Cilia length is positively correlated with eugenol absorption (linear regression fitting: $y = 35.8x – 167.8$; r = Pearson correlation).

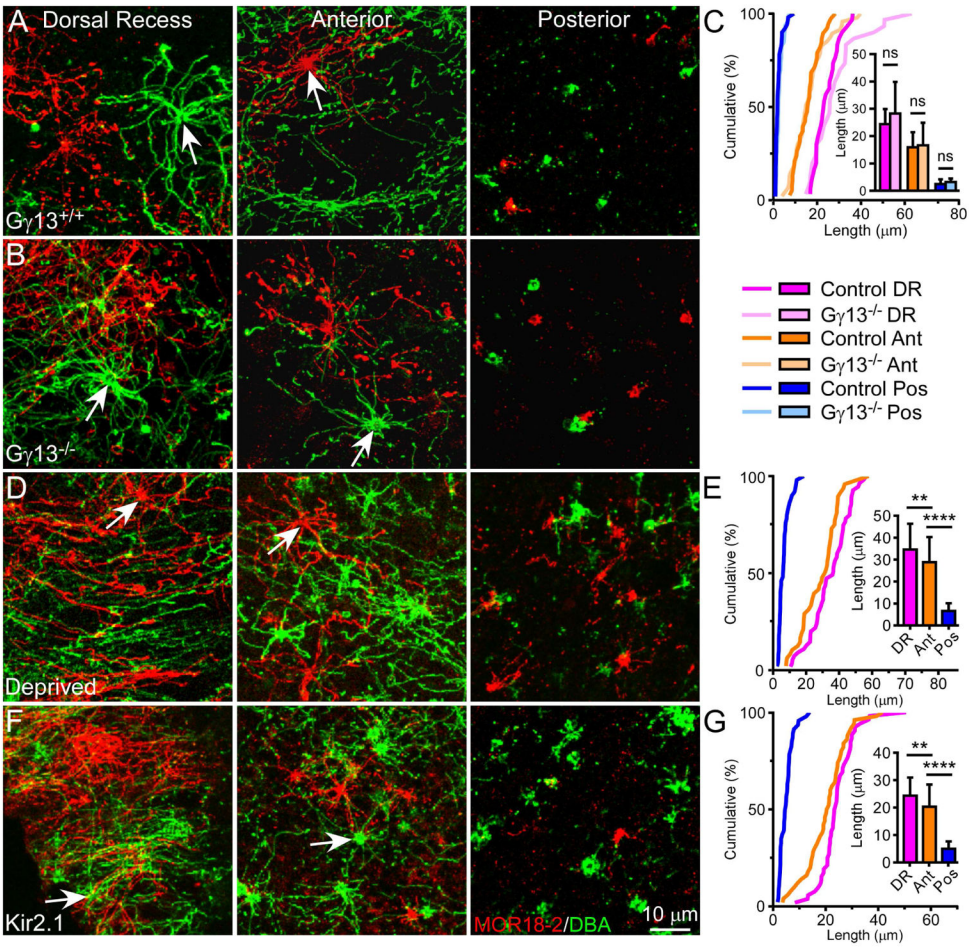

Figure 4. The Cilia Pattern Is Established by an Activity-Independent Mechanism

(**A** and **B**) Whole-mount olfactory epithelia from Gγ13 littermate controls (**A**) and Gγ13$^{-/-}$ mice (**B**) (n = 3 animals per genotype) were stained with MOR18-2 (red) and DBA (green). Confocal images were taken from the dorsal recess, anterior, and posterior septum. Arrows mark dendritic knobs. (**C**) Cumulative frequency (%) of cilia length from MOR18-2 cells in different regions. The bar graph shows quantification of cilia length (mean ± SD); Tukey's multiple comparisons test, ns – not significant. (**D**) Four weeks after naris closure (n = 8 animals), during which one nostril is deprived of both airflow and odorant influx, the olfactory epithelium was stained and imaged as in (A). (**E**) Cumulative frequency (%) of cilia length from MOR18-2 cells in different regions in the deprived side. The bar graph shows quantification of cilia length (mean ± SD); Tukey's multiple comparisons test, ** $p < 0.01$, **** $p < 0.0001$. Cilia are slightly longer in all regions compared to un-manipulated controls (see also Figure 2 and Tables S1 and S2), which may be attributed to multiple factors like better protection from physical damage and alterations in cell dynamics (i.e., OSN maturation stages), microenvironment, and/or expression of signaling molecules including upregulation of ACIII [44, 45] (see *Discussion*). (**F**) Whole-mount olfactory epithelia from Kir2.1 transgenic mice (n = 3 animals) were stained and imaged as in (A). Scale bar in (F) applies to all images. In these mice, olfactory marker protein (OMP) drives the expression of the inward rectifying K^+ channel Kir2.1, which results in dampened

neuronal excitability in mature OSNs but does not affect the upstream olfactory signal transduction events. (**G**) Cumulative frequency (%) of cilia length from MOR18-2 cells in different regions in Kir2.1 mice. The bar graph shows quantification of cilia length (mean ± SD); Tukey's multiple comparisons test, ** $p < 0.01$, **** $p < 0.0001$. See also Table S2.

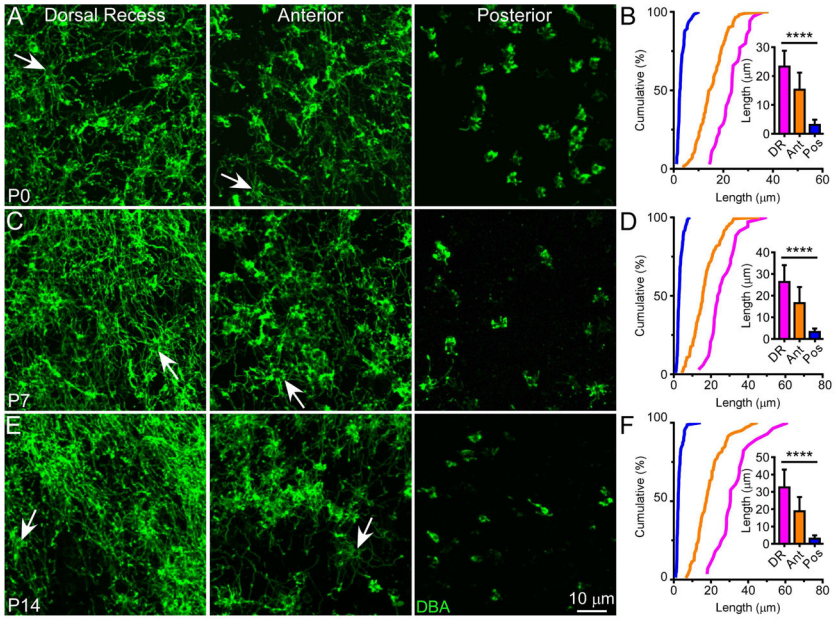

Figure 5. The Cilia Pattern Is Evident Throughout Postnatal Development

Whole-mount olfactory epithelia were stained with DBA at P0 (**A**), P7 (**C**), and P14 (**E**). Scale bar in (E) applies to all images. Arrows mark dendritic knobs. (**B**, **D**, and **F**) Cumulative frequency (%) of cilia length from DBA^+ cells in all three regions at different ages. The bar graph shows quantification of cilia length (mean ± SD); Tukey's multiple comparisons test, **** $p < 0.0001$. See also Figure S3 and Table S2.

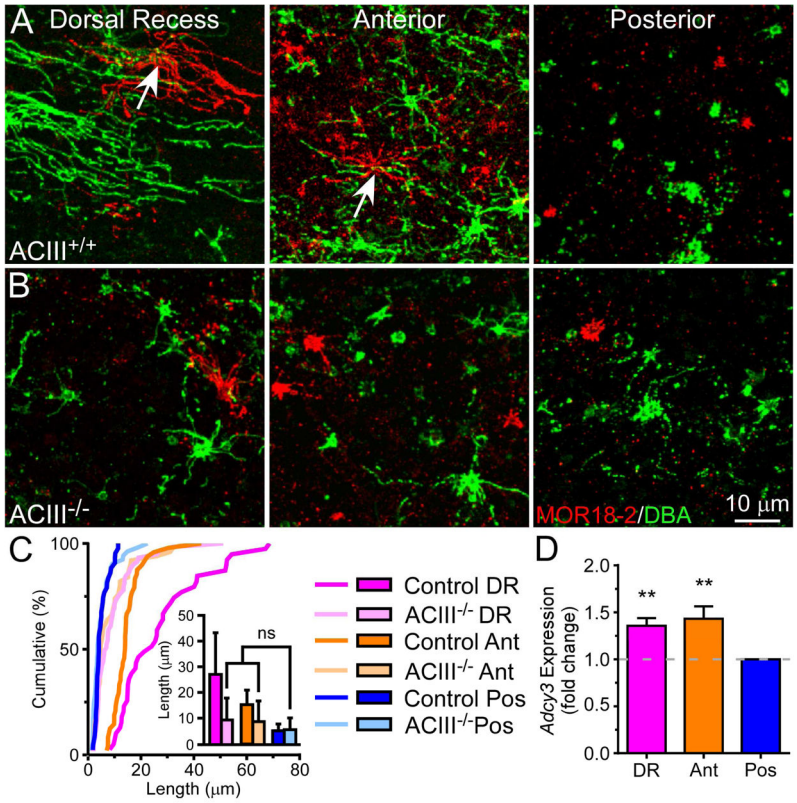

Figure 6. Genetic Ablation of ACIII Disrupts the Cilia Pattern

(**A** and **B**) Whole-mount olfactory epithelia from ACIII$^{+/+}$ (n = 4 animals) (**A**) and ACIII$^{-/-}$ mice (n = 6 animals) (**B**) were stained with MOR18-2 (red) and DBA (green). Scale bar in (B) applies to all images. Arrows mark dendritic knobs. (**C**) Cumulative frequency (%) of cilia length from DBA^{+} cells in different regions. The bar graph shows quantification of cilia length (mean ± SD); Tukey's multiple comparisons test, ns – not significant. See also Table S2. On average, cells in all regions possess 6.7 ± 2.8 cilia (n = 50 cells), similar to that observed in the posterior septum of wild-type mice (see *Results*). (**D**) *Adcy3* gene expression in wild-type olfactory epithelia (n = 3 animals and 3 replicates per animal) was measured using qRT-PCR and normalized to *Omp* expression. *Adcy3* expression (mean fold change ± SD) in the dorsal recess and anterior regions relative to the posterior septum: DR, 1.36 ± 0.08; Ant, 1.43 ± 0.13; one-way ANOVA, Dunnett's multiple comparisons test, F = 20.2, ** $p < 0.01$.

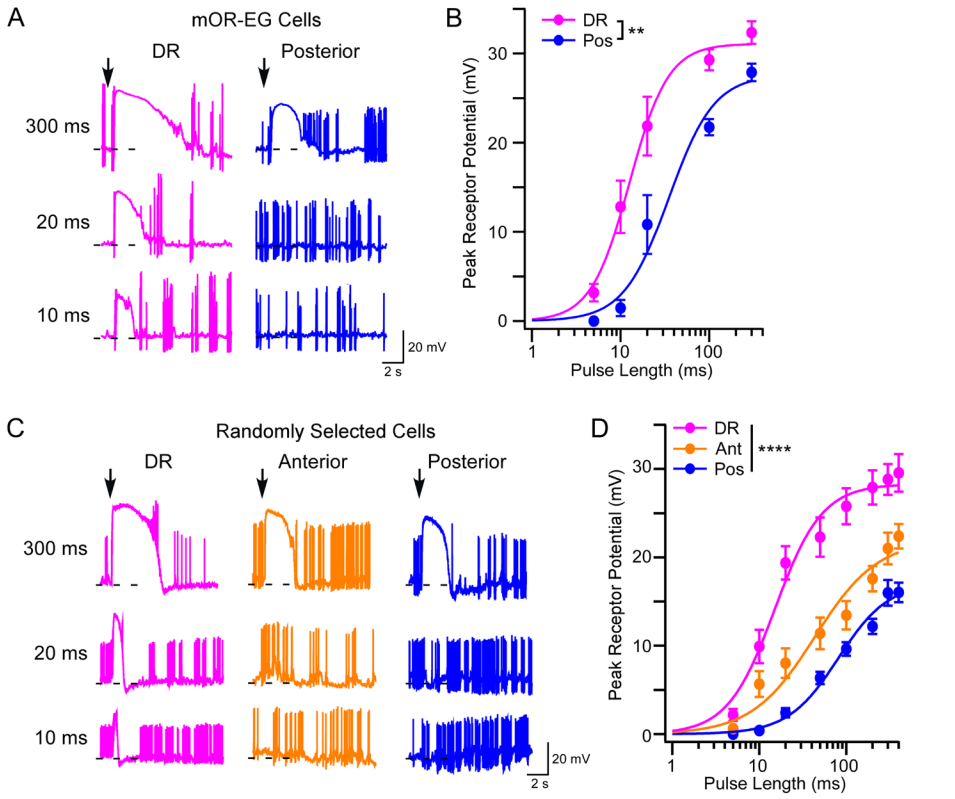

Figure 7. OSNs with Longer Cilia Are More Sensitive to Odorants

(**A**) Representative traces from mOR-EG cells recorded alternately from the dorsal recess (n = 10 cells) and posterior (n = 9 cells) septum under current clamp mode. To stimulate cells with different eugenol concentrations, we delivered pressure pulses at different lengths (up to 400 ms) from a pipette containing 10 μM eugenol. Arrows mark the onset of the stimuli and dashed lines indicate −60 mV. (**B**) Summary of eugenol-induced responses (mean ± SE). Dose response curves are fit with the Hill equation. $K_{1/2}$ is 12.7 and 35.0 ms for cells in the dorsal recess and posterior septum, respectively (two-way ANOVA, F = 3.2, ** $p < 0.01$). The dendritic knobs of mOR-EG cells in the anterior septum appeared smaller and slightly deeper from the surface, which made recordings from this region extremely difficult. In contrast, the dorsal recess has more cells to choose from and the posterior septum contains slightly bigger knobs. The anterior septum is included in randomly patched OSNs and in EOG recordings (see below). (**C**) Representative traces from randomly selected cells recorded from the dorsal recess (n = 28 cells), anterior (n = 31 cells), and posterior septum (n = 36 cells). We delivered pressure pulses as in (A) from a pipette containing a mixture of ten odorants (each at 10 μM). OR identity and ligand specificity were unknown since cells were arbitrarily chosen for recording. Therefore, approximately 50% of all recorded cells showed odorant-induced responses. (**D**) Summary of odor-induced responses from randomly selected cells. $K_{1/2}$ is 15.1, 43.4, and 80.8 ms for cells in the dorsal recess, anterior and posterior septum, respectively (two-way ANOVA, F = 6.3, **** $p < 0.0001$). Randomly selected cells showed lower sensitivity than mOR-EG cells because some OSNs were only weakly stimulated by the odorant mixture. The difference in response sensitivity

between anterior and posterior cells was further validated using EOG recordings (see also Figure S4).